Electronic Supplementary Material (ESI) for ChemComm.
This journal is © The Royal Society of Chemistry 2021

Electronic Supplementary Information

In vivo Monitoring of Volatile Metabolic Trajectories Enables Rapid Diagnosis of Influenza A Infection

Zhihong Yin,[ab] Wenbo Huang,[c] Kapil Dev Singh,[de] Zhaoming Chen,[c] Xing Chen,[ab] Zhen Zhou,[ab] Zifeng Yang *[cfg] Pablo Sinues *[de] and Xue Li *[ab]

[a] Institute of Mass Spectrometry and Atmospheric Environment, Jinan University, Guangzhou 510632, China

[b] Atmospheric Pollution Online Source Analysis Engineering Research Center of Guangdong Province, Jinan University, Guangzhou 510632, China

[c] State Key Laboratory of Respiratory Disease, National Clinical Research Center for Respiratory Disease, Guangzhou Institute of Respiratory Health, The First Affiliated Hospital of Guangzhou Medical University, Guangzhou 510120, China

[d] University Children's Hospital Basel, Basel 4056, Switzerland

[e] Department of Biomedical Engineering, University of Basel, Basel 4056, Switzerland

[f] Faculty of Chinese Medicine, Macau University of Science and Technology, Taipa 999078, PR China

[g] KingMed Virology Diagnostic & Translational Center, Guangzhou 510320, PR China

*E-mail of the correspondence author: tamylee@jnu.edu.cn (X. Li), pablo.sinues@unibas.ch (P. Sinues), jeffyah@163.com (Z. Yang)

Contents

S1. Materials and Methods

S1.1 Virus infection models

Female BALB/C mice 6–8 weeks old were purchased from Guangdong Medical Laboratory Animal Center (Guangzhou, China). The mice were housed in specific pathogen free facilities, bred, and genotyped according to the vendor's protocols. The mice were divided into four groups, i.e., IAV infected mice (IAV group), healthy control mice (Mock group), IAV infected combined with oseltamivir treatment mice (OSE group) and inactivated IAV treated mice (Inactivated IAV group) (Fig. S1a). For the IAV and OSE groups, mice anesthetized with 2.5% isoflurane were inoculated intranasally with 50 μL of 2LD50 (50% lethal dose) IAV (H1N1); the OSE group were orally administered with oseltamivir phosphate (Stru Chem Co., Ltd, China) (60 mg/kg/d) on the day of infection as well as the following four days. In case of mock and inactivated IAV groups, phosphate buffered saline (PBS) and inactivated IAV were treated with the healthy mice, respectively. To monitor viral titers in lungs and histology, mice were sacrificed by euthanasia at 1, 3, 5 and 7 days post infection. At each time point, the lungs from 5 mice per group were collected for the detection of the viral titer. The lungs from 2 mice were fixed with 10% neutral formalin for histopathological examination. All the animal experiments were performed in compliance with Chinese Animal Protection Act and the National Research Council Criteria; the study has been approved by the Laboratory Animal Ethics Committee of Affiliated First Hospital of Guangzhou Medical University (No.2019120).

S1.2 Measurement of viral titer

Lung samples were homogenized in 1 mL of sterile PBS. Madin-Darby canine kidney (MDCK) cells were inoculated with tenfold serial dilutions of lung homogenates in 96-well plates. After 1 h incubation, the suspension was removed, and the cells were cultured in minimum Eagle's medium (MEM), including 2 μg/mL trypsin. The cells were incubated for 2–3 days at 37 °C with 5% CO_2. The presence of cytopathic effects

(CPE) was determined under a microscope, and viral titers were calculated by using the Reed-Muench method.

S1.3 Hematoxylin and eosin (H&E) staining

As soon as the lung samples were obtained, they were immediately fixed in 10% formalin, embedded in paraffin and sectioned (4 μm thickness) for histopathologic analysis. The sections were stained with hematoxylin and eosin (H&E) for examination by light microscopy.

S1.4 Real-time *in vivo* measurement of mouse breath

Mouse was placed in a 50-mL Falcon tube and the volatile metabolites was delivered through a PTFE tube (6 mm od) into a SESI source (Super SESI, FIT, Spain) by clean dry air (without VOCs) at a steady flow rate of 1 L/min (Fig. S1b). VOC-free air was produced by a zero air generator (Beijing anjiehua Co., Ltd; Beijing, China). Sample firstly passed through a particle filter (Sensabues, Sweden) and then was delivered into the source *via* a sampling line heated at 130 °C. Ions formed in the SESI source were detected by a high-resolution quadrupole orbitrap mass spectrometer (Thermo Scientific Q-Exactive Orbitrap MS, Waltham, MA USA) in positive and negative modes with spray voltages set to +2.5 kV and −2.5 kV, respectively. Nano-ESI spray solution was 0.1% formic acid water. Ion transfer capillary temperature was 275 °C. The mass range was *m/z* 50–500 and the resolution was set to 70,000 (at *m/z* 200).

For individual mice, it took ≤ 30 min for each measurement and all the mice were measured at the same time everyday post infection. The experimental period has covered the course of the infection till the inoculated mice died. Mouse health status, e.g., body weight, was recorded on the same day of the measurement. All the mice were given free access to the food and water during the 9-day experimental Considering the volatile compounds emitted from mouse feces may influence the

results, the mice were deprived of food and water for 2–3 hours before administration to minimize the production of feces; clean tissues were placed at the rear of the mouse to absorb urine and feces; trimethylamine (TMA), a volatile maker of feces, was monitored and the data were aborted if a significant increase in TMA intensity was observed.[1]

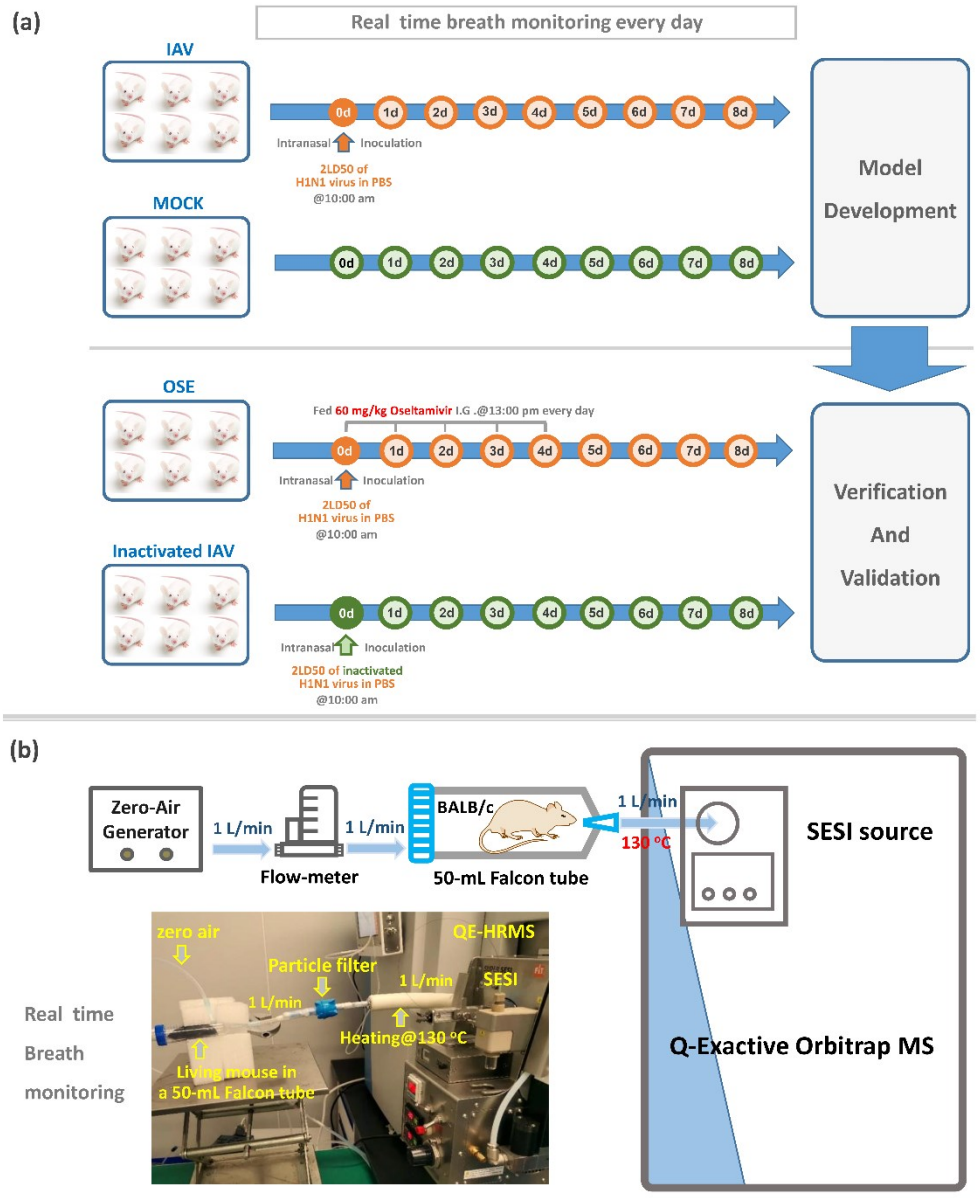

Fig. S1 (a) Experimental design for monitoring IAV infection in living mice by volatile metabolites within the 9-day experimental period. (b) Schematic of real time *in vivo* monitoring of volatile metabolites emitted from mice by SESI-HRMS.

S1.5 Data Pre-processing

Raw mass spectra (Thermo's proprietary RAW format) were converted into mzXML format using Proteowizard (command line tool *msconvert*). All subsequent analysis was performed using MATLAB. 20 scans per file were firstly interpolated using a shape-preserving piecewise cubic interpolation method (range *m/z* 50–500; linearly spaced steps of 10^{-4} Da). This resulted in 404 continuous mass spectra. Fig. S2 shows a zoom of the resulting 202 spectra (positive mode) at *m/z* 255.

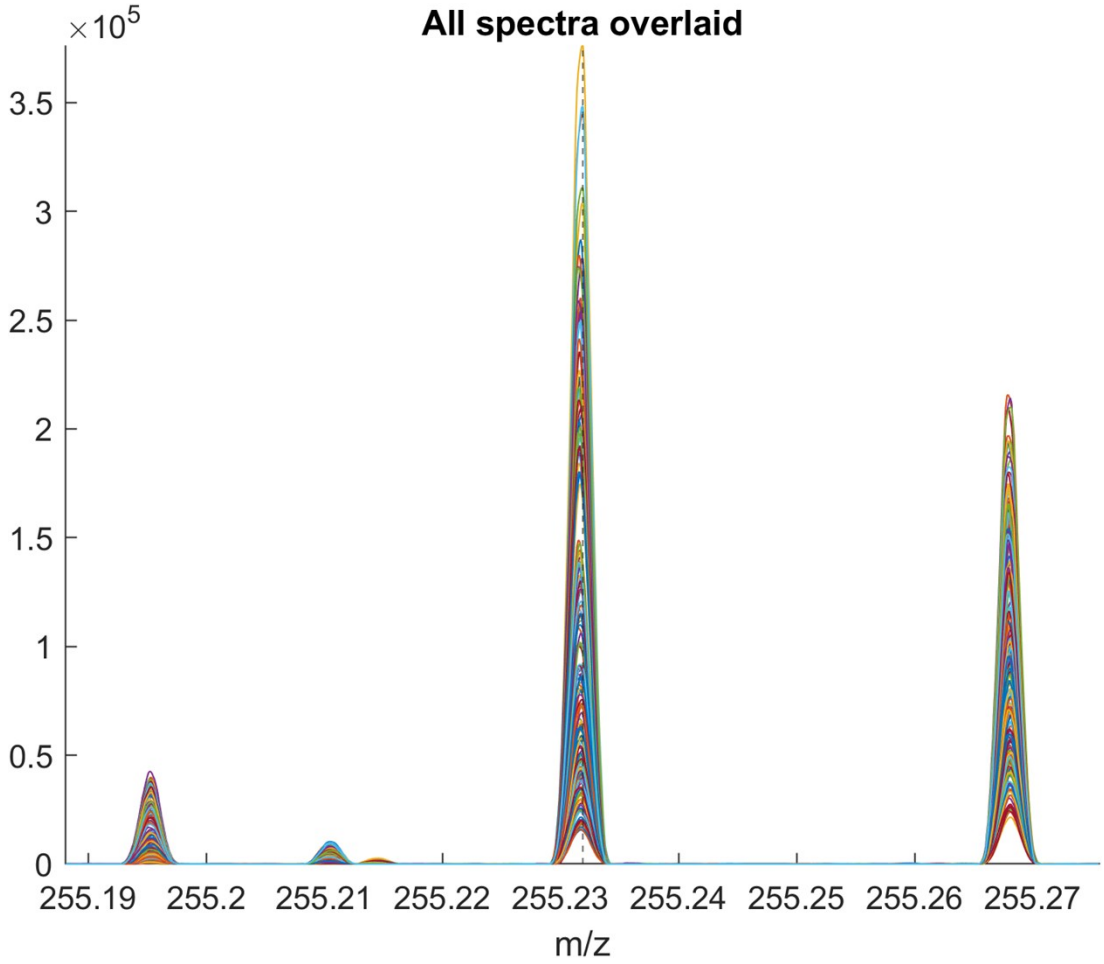

Fig. S2 Peak alignment and calibration. Zoom of the resulting 202 spectra (positive mode) at *m/z* 255. Note how the spectra is aligned and calibrated (reference dashed line corresponds to $[C_{16}H_{30}O_2]^+$; *m/z* 255.2319).

These continuum mass spectra were then centroided using a peak intensity threshold of 5,000 a.u. The centroided *m/z* values were binned by constructing a Kernel density function over the histograms of this centroid *m/z* list, with the appropriate band width to match the theoretical instrument resolution (70,000 at *m/z* 200, but scaling as a function of the inverse of the square root of *m/z*; Fig. S3). Fig. S4 displays an example of the histogram of the mass list and their corresponding Kernel density function at *m/z* 255. The Kernel density functions were then centroided, resulting in a final list of 3,655 features (2,854 in positive mode and 801 in negative mode). Finally, to generate the final data matrix, we computed the signal intensity for each of these features for each sample. To do so, we summed the signal intensity of the interpolated spectra at FWHM of these 3,655 features. This resulted in a final data matrix of 202 samples x 3,655 mass spectral features. The number one was added to the matrix to avoid zero signal intensities and hence infinity when further computing ratios. All data points for each of the 24 mice were divided by the signal intensity of the first day (i.e. inoculation day 0) and the $\log_2$ fold change (FC) were computed (with respect to the first day).

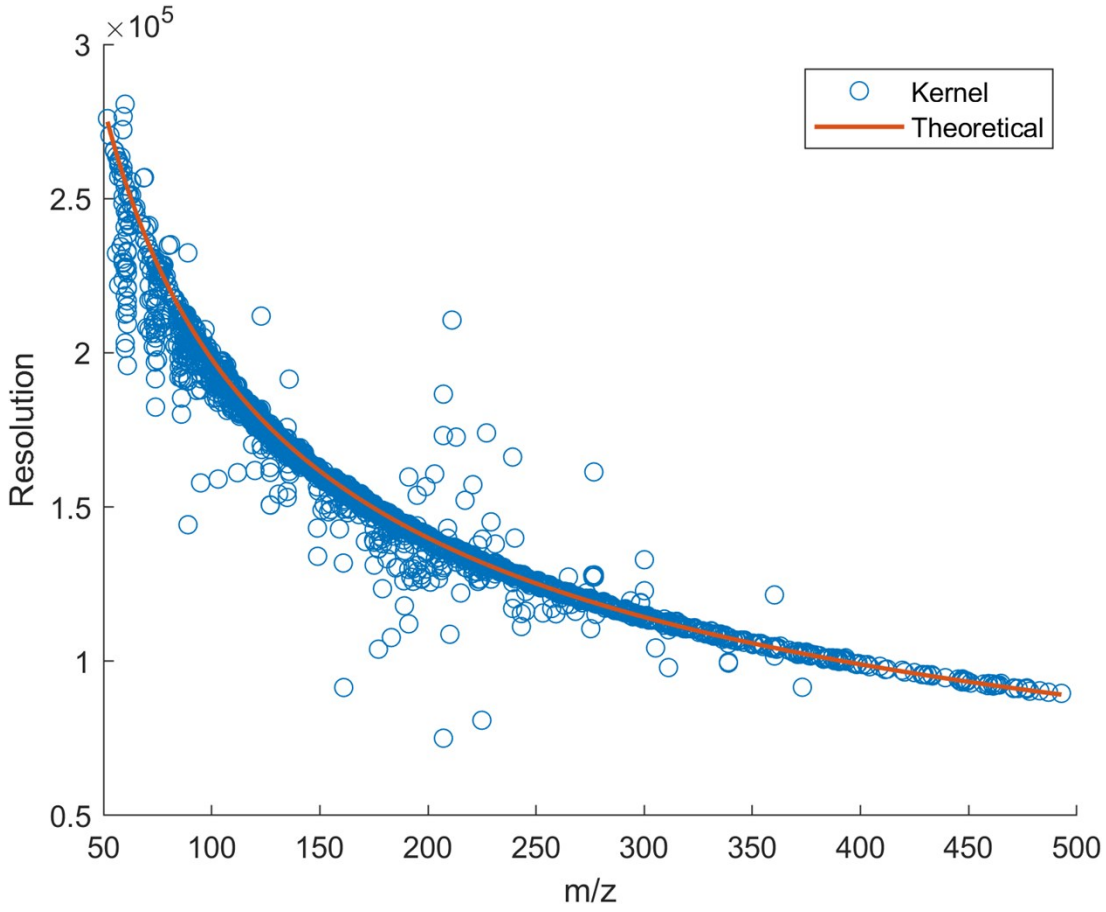

Fig. S3 The centroided *m/z* values were binned by constructing a Kernel density function over the histograms of this centroid *m/z* list, with the appropriate band width to match the theoretical instrument resolution (70,000 at *m/z* 200, but scaling as a function of the inverse of the square root of *m/z*).

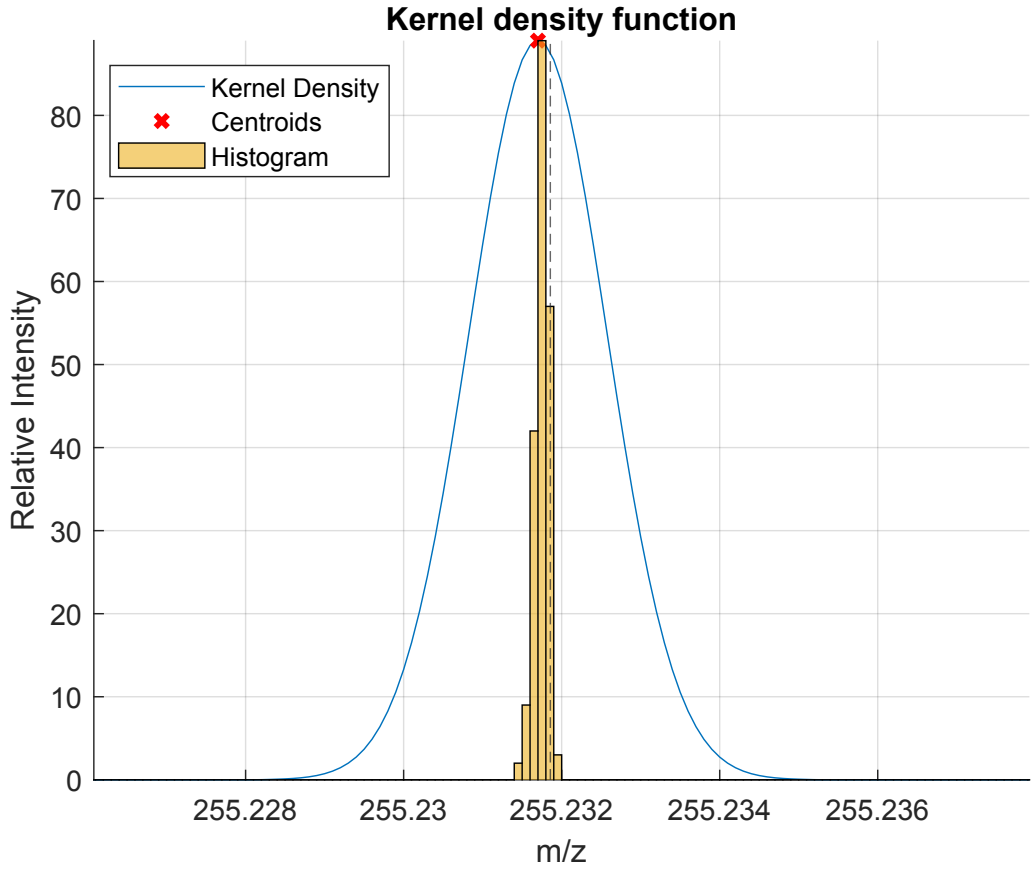

Fig. S4 An example of the histogram of the mass list and their corresponding Kernel density function at *m/z* 255.232.

S1.6 Data Post-processing

The 202 x 3,655 data matrix of $\log_2$ FC intensity values was subdivided into the one containing the IAV and mock groups (94 samples x 3,655 features) and a second submatrix containing the data for the OSE and inactivated IAV groups(108 samples x 3,655 features). The first matrix (IAV and mock groups) was utilized to identify metabolites potentially associated to the infection. The second matrix (OSE and inactivated IAV groups) was reserved for validation purposes.

In order to determine which features varied over time for the infection group differently from the control group, we applied a repeated measures ANOVA (RANOVA) test. Ions with a significant (*i.e. p*-value with Lower bound adjustment <

0.05) effect of time on ion signal intensity and significant (*i.e. p*-value with Lower bound adjustment < 0.05) group-time interaction, were further considered.

The IAV and mock groups' data matrix comprising only the RANOVA-significant features was then subjected to Principal Component Analysis (PCA) after mean-centering. Subsequently, the OSE and inactivated IAV data matrix was projected onto this model (generated exclusively by the IAV and mock groups) to determine whether a similar pattern emerged.

Finally, we attempted to predict the OSE and inactivated IAV during the course of infection. To do so, we trained a support vector machine (SVM) model using the first two PCA scores of the IAV and mock groups' data matrix (previously filtered by RANOVA). The model was then used to predict the projected first two scores of the OSE and inactivated IAV data. Again, please note that none of the OSE and inactivated IAV data was used for model building, hence minimizing the bias.

S1.7 Metabolic pathway enrichment analysis

Accurate *m/z*, *p*-value with Lower bound adjustment and *t*-score were used to compute pathway enrichment using R package MetaboAnalystR (version 2.0.4).[2] Analysis was performed as per "MS Peaks to Pathways" module of MetaboAnalystR with following settings: mass accuracy = 2 ppm, instrument mode = mixed, method version = v1, organism library = mmu_kegg, library version = current, Mummichog *p*-value cutoff = 0.001 and permutation number = 1000. Additionally, we used custom adducts for positive (M+H [1+], M(C^{13})+H [1+], M−H_2O+H [1+], M−NH_3+H [1+], M+NH_4 [1+]) and negative (M−H [1−], M(C^{13})−H [1−], M−H_2O−H [1−]) modes.

S2. Results

S2.1 Physiological characterization of viral infection

The virus replication peaked at 3 dpi among virus infected mice treated with or without oseltamivir, with decrease trends from 5 to 7 dpi. (Fig. S5a). We further examined the histopathologic changes in the lungs of the mice. At 1 dpi, virus infected-mice showed interstitial pneumonia in the lung area adjacent to bronchioles, which became more severe with lymphocytic infiltration at 3 dpi. At 5 and 7 dpi, the lesion extended to a larger area of lung. The histopathologic changes in the lungs of oseltamivir treated-mice were much milder with reduced infiltration of inflammatory cells. (Fig. S5b).

IAV group mice systematically lost weight from 2 dpi and weight loss reached maximal value (28.0±5.7%) at or before 9 dpi (Fig. S5c), showing a clear indication of infection development. In contrast, the mock group mice systematically gained weight, especially during the first two days. Regarding OSE and inactivated IAV groups, a similar situation was found, although the differences between the two groups were not stark, as expected. The OSE group almost resembled the IAV group except that a sharp drop in body weight in OSE group was delayed to 3–4 dpi. The delay was probably caused by the effect of the antiviral therapy, which was administered during the first five days of the experiment. However, the treatment failed to ultimately prevent critical infection, as evidenced by the loss weight experienced by five mice (32.4±2.4% at 9 dpi) (Fig. S5c). Interestingly, one mouse in the OSE group recovered weight post treatment with the antiviral medication (solid trace with triangles in right panel of Fig. S5c).

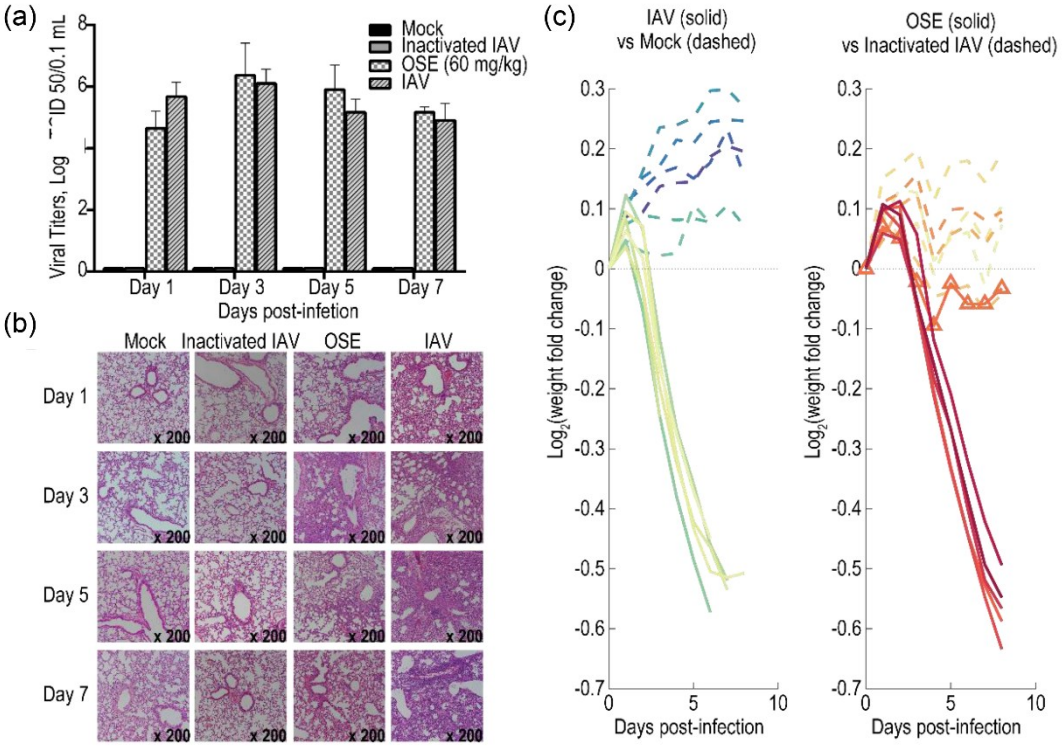

Fig. S5 Devastating impact of the infection over time. (a) The mean lung virus titers (±SD) recovered from mice (n=5) of different groups at 1, 3, 5 and 7 dpi. (b) The histological injuries in the lungs of different groups. The lung tissues were harvested immediately after the mice were executed on day post infection1, 3, 5 and 7, and the lung sections were prepared and stained with HE; Original magnification: x 200. (c) Change in body weight during the course of infection represented as log2(Fold change of weight). The solid trace with triangles corresponds to one mouse in the OSE group that showed a different response to the rest of the group.

S2.2 Altered metabolic pathways as captured by real-time analysis

Table S1 Comparison of top 40 metabolic pathways altered by H1N1 virus infection captured in mouse breath in this study with pathways reported in other studies.

No.	Pathway	Total_Size	Hits	Combined_Pvals	Class	A549 Cells[†]	Mice[‡]	Ferrets[§]
1	Glyoxylate and dicarboxylate metabolism	31	14	0.00001	Carbohydrate metabolism			
2	Alanine, aspartate and glutamate metabolism	28	17	0.00021	Amino acid metabolism	√	√	√
3	Nitrogen metabolism	6	4	0.00052	Energy metabolism	√		
4	Purine metabolism	66	5	0.00055	Nucleotide metabolism	√	√	
5	Arginine biosynthesis	14	10	0.00167	Amino acid metabolism			
6	Propanoate metabolism	19	8	0.00195	Carbohydrate metabolism			
7	Glycerolipid metabolism	7	4	0.00905	Lipid metabolism			
8	D-Glutamine and D-glutamate metabolism	6	6	0.01262	Metabolism of other amino acids	√		
9	Citrate cycle (TCA cycle)	16	6	0.01913	Carbohydrate metabolism		√	
10	Fatty acid degradation	36	2	0.02419	Lipid metabolism			
11	Pyruvate metabolism	19	9	0.03753	Carbohydrate metabolism			
12	Sphingolipid metabolism	9	5	0.03901	Lipid metabolism			
13	Butanoate metabolism	15	9	0.05935	Carbohydrate metabolism	√		
14	Arginine and proline metabolism	37	25	0.1126	Amino acid metabolism	√	√	√
15	Pyrimidine metabolism	39	9	0.121	Nucleotide metabolism	√	√	
16	Galactose metabolism	27	10	0.136	Carbohydrate metabolism	√		
17	Tyrosine metabolism	42	32	0.1563	Amino acid metabolism			√
18	Biosynthesis of unsaturated fatty acids	34	10	0.1682	Lipid metabolism			
19	Glycine, serine and threonine metabolism	31	20	0.1686	Amino acid metabolism	√	√	√
20	Cysteine and methionine metabolism	33	8	0.1946	Amino acid metabolism	√		
21	Fatty acid elongation	30	1	0.2372	Lipid metabolism			
22	Glycolysis / Gluconeogenesis	23	6	0.2448	Carbohydrate metabolism			
23	Selenocompound metabolism	16	2	0.3207	Metabolism of other amino acids			

24	Inositol phosphate metabolism	21	2	0.3986	Carbohydrate metabolism			
25	Synthesis and degradation of ketone bodies	5	2	0.4017	Lipid metabolism			
26	Glutathione metabolism	19	6	0.4162	Metabolism of other amino acids	√		
27	Ubiquinone and other terpenoid-quinone biosynthesis	9	3	0.5183	Metabolism of cofactors and vitamins			
28	Porphyrin and chlorophyll metabolism	27	3	0.5648	Metabolism of cofactors and vitamins	√		
29	Drug metabolism - other enzymes	27	3	0.5648	Xenobiotics biodegradation and metabolism			
30	Fructose and mannose metabolism	18	6	0.5999	Carbohydrate metabolism	√		
31	Primary bile acid biosynthesis	46	8	0.6102	Lipid metabolism	√		
32	Terpenoid backbone biosynthesis	15	2	0.6594	Metabolism of terpenoids and polyketides			
33	beta-Alanine metabolism	21	9	0.6667	Metabolism of other amino acids	√		
34	Valine, leucine and isoleucine degradation	35	12	0.7194	Amino acid metabolism			
35	Aminoacyl-tRNA biosynthesis	22	16	0.7198	Genetic Information Processing; Translation	√		
36	Phenylalanine metabolism	12	10	0.7426	Amino acid metabolism			√
37	Fatty acid biosynthesis	10	5	0.7749	Lipid metabolism	√		
38	Glycerophospholipid metabolism	13	3	0.8027	Lipid metabolism	√		
39	Valine, leucine and isoleucine biosynthesis	8	7	0.8467	Amino acid metabolism			√
40	Histidine metabolism	16	13	0.8807	Amino acid metabolism	√	√	

[†][3]; [‡][4]; [§][5].

S3. References

1 X. Chen, K. D. Zhang, Z. H. Yin, M. L. Fang, W. D. Pu, Z. N. Liu, L. Li, P. Sinues, R. Dallmann, Z. Zhou and X. Li, Anal. Chem. 2021, DOI: 10.1021/acs.analchem.1c00509.

2 W. Q. Pan, Z. Y. Dong, F. Li, W. X. Meng, L. Q. Feng, X. F. Niu, C. F. Li, Q. F. Luo, Z. F. Li, C. J. Sun and L. Chen, *Nat. Commun.,* 2013, **4**, 2369.

3 X. D. Tian, K. Zhang, J. Min, C. Chen, Y. Cao, C. Ding, W. J. Liu and J. Li, *Viruses-Basel,* 2019, **11**, 1007.

4 J. D. Chandler, X. Hu, E. J. Ko, S. Park, Y. T. Lee, M. Orr, J. Fernandes, K. Uppal, S. M. Kang, D. P. Jones and Y. M. Go, *Am. J. Physiol-Reg. I.,* 2016, **311**, R906-R916.

5 D. J. Beale, D. Y. Oh, A. V. Karpe, C. Tai, M. S. Dunn, D. Tilmanis, E. A. Palombo and A. C. Hurt, *Metabolomics,* 2019, **15**, 33.